Nanosurface Energy Transfer from Long-Lifetime Terbium Donors to Gold Nanoparticles

Chi Chen, Clyde Midelet, Shashi Bhuckory, Niko Hildebrandt, Martinus H. V. Werts

THE JOURNAL OF PHYSICAL CHEMISTRY C

Article

Cite This: J. Phys. Chem. C 2018, 122, 17566−17574

pubs.acs.org/JPCC

Nanosurface Energy Transfer from Long-Lifetime Terbium Donors to Gold Nanoparticles

Chi Chen,[†,§] Clyde Midelet,[‡,§] Shashi Bhuckory,[†] Niko Hildebrandt,*[,†] and Martinus H. V. Werts*[,‡]

[†]NanoBioPhotonics (nanofret.com), Institute for Integrative Biology of the Cell (I2BC), Université Paris-Saclay, Université Paris-Sud, CNRS, CEA, 91400 Orsay, France

[‡]Univ Rennes, CNRS, SATIE-UMR8029, École normale supérieure de Rennes, Campus de Ker Lann, F-35170 Bruz, France

Supporting Information

ABSTRACT: Photoluminescence (PL) quenching by gold nanoparticles (AuNPs) is a frequently applied principle in nanobiosensing. The quenching is most often explained in terms of the Förster resonance energy-transfer (FRET) mechanism, and more rarely in terms of the nanosurface energy-transfer (NSET) mechanism. Although both consider nonradiative resonance energy transfer, there are significant differences in predictions of the strength and the distance-dependence of the quenching. Here, we investigate the energy transfer to AuNPs from a terbium(III)-complex (Tb) with a long (millisecond) PL decay time with the aim to provide a better understanding of the underlying energy-transfer process. The binding of Tb-labeled streptavidin (Tb-sAv) to biotinylated AuNPs (biot-AuNPs) was studied using light-scattering spectroscopy. Quenching of the PL of Tb-sAv upon binding to biot-AuNPs of different diameters (5, 30, 50, 80 nm) was studied by time-resolved PL spectroscopy. Energy-transfer efficiencies were found to be practically independent of the AuNP size. Analysis according to FRET theory yielded donor−acceptor distances that were inconsistent and far beyond the expected Tb−AuNP distance. In contrast, the NSET model yielded a good agreement between the Tb-to-AuNP surface distance estimated from the geometry of the Tb-sAv/biotin-AuNP assembly (4.5 nm) and those calculated from PL lifetime analysis, which range from 4.0 to 6.3 nm. Our findings strongly suggest that NSET (and not FRET) is the operational mechanism in PL quenching by AuNPs, which is important information for the development, characterization, and application of nanobiosensors based on PL quenching by AuNPs.

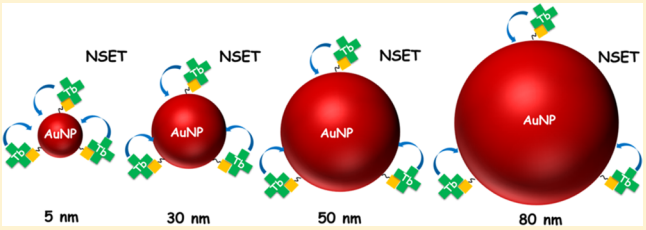

The application of excitation energy transfer has expanded the applicability of luminescent probe methodologies in biochemistry, clinical diagnostics, and biomolecular imaging.[1−3] The understanding of the energy-transfer mechanism between donors and acceptors plays a fundamental role in developing and optimizing biosensing technologies. Förster resonance energy transfer (FRET) is the best-known energy-transfer mechanism and has been confirmed for pairs of small donor and acceptor molecules. It predicts the energy-transfer efficiency to be inversely proportional to the sixth power of the distance between the donor and the acceptor.[4] This energy transfer occurs at intermolecular distances in the small window between approximately 1 and 20 nm,[5] a range that is ideally suited for observing dynamic biomolecular interactions, involving proteins, nucleic acids, cell membranes, and other biological systems.[6] However, many biomolecular processes take place over longer distances, and their dynamic interactions are difficult to follow by FRET. Thus, investigating and understanding longer-range energy-transfer processes and using them for biosensor development is highly desirable.

Theorized by Persson and Lang,[7] nanosurface energy transfer (NSET) has emerged as an energy-transfer mechanism that can measure biomolecular interactions over distances up to 50 nm and thereby more than double the range of FRET.[8] Similar to FRET, NSET is a nonradiative dipole−dipole energy transfer, but in contrast to FRET (in which both donor and acceptor are considered as point dipoles), the acceptor is a nanometric surface modeled as a collection of many dipoles. In NSET, the efficiency is inversely proportional to the fourth power of the distance between the donor and the acceptor surface of a metallic nanoparticle (NP) (in most cases AuNPs).[9,10] Research showed that NSET model was in good agreement with the experimental data on small-size AuNPs (below 3 nm) in combination with organic dyes and quantum dots (QDs) as donors.[10−12] NSET behavior with energy-transfer efficiencies independent of the NP size or number of donors was also demonstrated for larger-size AuNPs.[13−16] However, in other studies reporting about biosensors that use photoluminescence (PL) quenching by AuNPs, the underlying energy-transfer mechanism is assumed to be FRET,[17,18] or is not specified.[19,20]

Studies of the NSET mechanism have focused on the interaction of AuNPs with organic dyes and QDs but have as

Received: July 9, 2018
Published: July 24, 2018

DOI: 10.1021/acs.jpcc.8b06539
J. Phys. Chem. C 2018, 122, 17566−17574

yet not used luminescent lanthanide complexes as the energy donor. Although hybrid nanomaterials incorporating luminescent lanthanide ions and plasmonic AuNPs have been reported in the literature,[21−23] a quantitative experimental study on the applicability of NSET versus FRET mechanisms in these materials has not been carried out. In comparison to the fluorescent molecular energy transfer donors, lanthanide ions offer some distinctive features such as long excited-state lifetimes (in the micro- to millisecond range) and multiple narrow emission bands in the visible region of the spectrum.[24] Thus, the investigation of lanthanide-to-AuNP energy transfer with AuNPs of different sizes has the potential to provide new insight for the debate on whether FRET or NSET is the cause of AuNP-based PL quenching.

In the present study, we investigated the energy-transfer interactions between Tb and AuNPs in assemblies of Tb-labeled streptavidin (Tb-sAv) with biotinylated AuNPs (biot-AuNPs) having diameters of 5, 30, 50, and 80 nm (Figure 1).

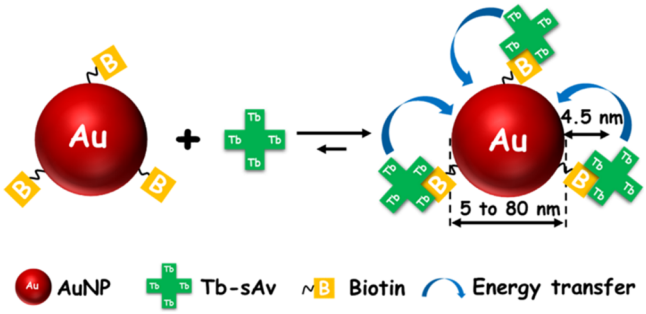

Figure 1. Schematic representation (not to scale) of the assemblies of Tb-labeled sAv (Tb-sAv) and biotinylated AuNPs (biot-AuNPs), wherein excitation energy transfer occurs. For clarity, only 3 biotins are shown. The actual number of biotins attached to the surface of each AuNP was determined to be ca. 25, 900, 2500, and 6400 for the 5, 30, 50, and 80 nm diameter AuNPs, respectively. A distance of 4.5 nm was estimated using a radius of 3 nm for sAv (size of sAv in the solid state: 5.4 nm × 5.8 nm × 4.8 nm in the solid state)[25] plus 1.5 nm for the biotin and linker attached to the AuNP.

Resonant light-scattering (RLS) spectroscopy and time-resolved PL spectroscopy were applied to characterize the different Tb-sAv/biot-AuNP assemblies at various donor−acceptor ratios. The PL decays of Tb-sAv/biot-AuNP assemblies at different concentrations and with AuNPs of all four diameters were studied by both stretched exponential (Kohlrausch) and multiexponential PL decay analyses. The energy-transfer efficiencies were found to be independent of the AuNP size. The NSET theory provided excellent agreement between the time-resolved PL results and the Tb-to-AuNP distances within the different Tb-sAv/biot-AuNP assemblies, whereas application of FRET theory led to unrealistically long Förster distances and Tb−AuNP distances without any correlation between different AuNP sizes. Our results strongly suggest that energy transfer between Tb and AuNPs is of NSET type, which is a very important finding for understanding and designing AuNP-based biosensors and assemblies of AuNPs with photoluminescent units.

RESULTS AND DISCUSSION

Characterization of Tb-sAv/biot-AuNP Assemblies. The number of binding sites for sAv on each nanoparticle is of the same order of magnitude as the number of biotins per particle. In principle, sAv can bind up to four biotins.[26] The number of biotins per biot-AuNP were given by the supplier as a number density of approximately 0.5 nm^{-2} at the AuNP surface. At the same time, the surface areas were given as 78.5, 2830, 7850, and 20 100 nm^2 for the 5, 30, 50, and 80 nm AuNPs, respectively, which led to 39 biotins per 5 nm AuNP, 1415 biotins per 30 nm AuNP, 3925 biotins per 50 nm AuNP, and 10 050 biotins per 80 nm AuNP. Because no explanation of this estimation was provided, we applied our own estimation based on the number of Au surface atoms, which we calculated to be 500 for 5 nm biot-AuNPs, 18 000 for the 30 nm biot-AuNPs, 50 000 for the 50 nm biot-AuNPs, and 128 000 for the 80 nm biot-AuNPs. Assuming the number of available biotins on the surface to be ca. 5% of the number of Au surface atoms led to 25 biotins per 5 nm biot-AuNP, 900 biotins per 30 nm biot-AuNP, 2500 biotins per 50 nm biot-AuNP, and 6400 biotins per 80 nm biot-AuNP, which were in good agreement with the estimates of the supplier. Taking into account that four biotins from the biot-AuNP will be able to bind one sAv, and ignoring any steric effects, the number of sAv that can bind to one nanoparticle is anticipated to be 6 for 5 nm biot-AuNPs, 225 for 30 nm biot-AuNPs, 625 for 50 nm, and 1600 for 80 nm biot-AuNPs. The PL titrations reported below enabled us to refine these estimates.

The interaction of Tb-sAv with biot-AuNPs was investigated by monitoring the light-scattering spectra[27,28] of the biot-AuNPs and introducing Tb-sAv into the solution. The light-scattering spectra consist of the localized surface plasmon resonance of AuNPs, which is sensitive to the environment of the particles. In particular, immobilization of biomolecules at the nanoparticle surface leads to small changes (a few nm) in the position of the maximum of these resonance bands. Larger shifts in the plasmon maximum (> 10 nm) are in general the result of clustering of AuNPs into aggregates, which leads to a strong coupling between the localized plasmon resonances of the individual particles.[27−30] The particular sensitivity of the resonant light-scattering spectrum toward the environment of the AuNPs provides a tool for monitoring the state of the biot-AuNPs when interacting with Tb-sAv.

Figure 2 shows the evolution of the wavelength of the maximum λ_{max} of the resonant light-scattering spectrum of biot-AuNPs (30, 50, 80 nm diameter) over time, before and after adding Tb-sAv to the solution. The light scattering by 5 nm AuNPs was too weak and not studied. The amount of Tb-sAv added was 25% of the amount needed to cover all binding

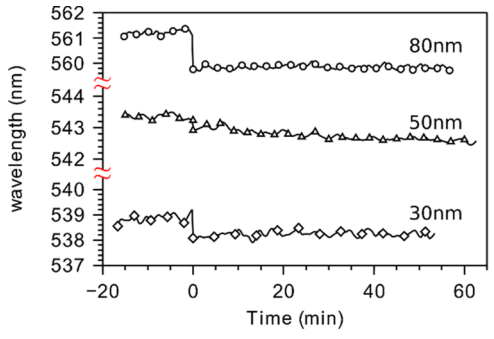

Figure 2. Wavelength evolution of the maximum of the resonant light-scattering band of biot-AuNPs (30, 50, and 80 nm diameter AuNPs) as a function of time. At t = 0, Tb-sAv (25% with respect to biot-AuNP binding sites) was added.

DOI: 10.1021/acs.jpcc.8b06539
J. Phys. Chem. C 2018, 122, 17566−17574

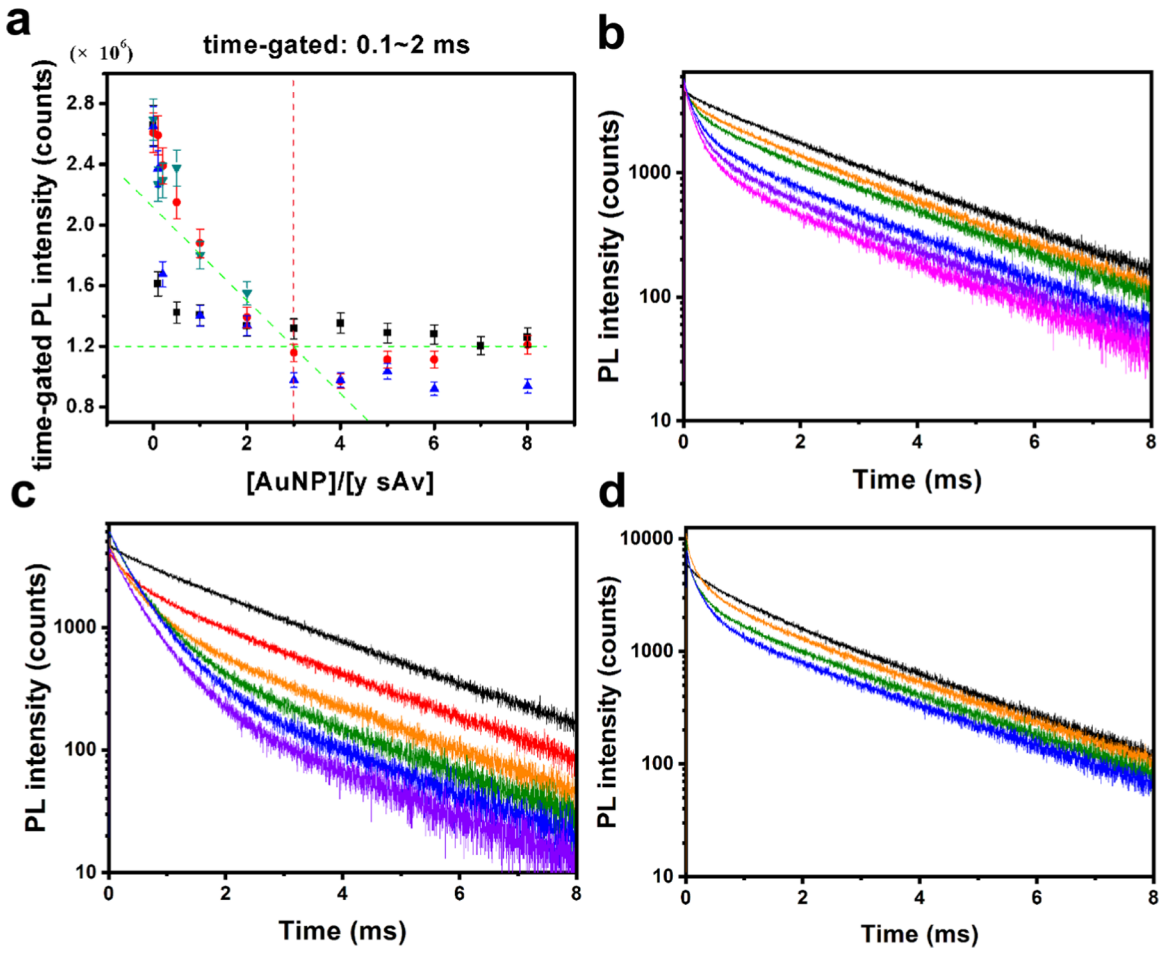

Figure 3. PL titration of Tb-sAv with biot-AuNP. (a) Integrated time-gated (0.1−2 ms) PL intensities of the PL decay curves (black: 5 nm biot-AuNPs; red: 30 nm biot-AuNPs; blue: 50 nm biot-AuNPs; and green: 80 nm biot-AuNPs). Crossing of the green dotted lines (at 3 [biot-AuNP]/[y Tb-sAv] with y = 6 for 5 nm biot-AuNPs, y = 225 for 30 nm biot-AuNPs, y = 625 for 50 nm biot-AuNPs, and y = 1600 for 80 nm biot-AuNPs) indicates the maximum number of Tb-sAv per biot-AuNP (6/3 = 2 for 5 nm biot-AuNPs, 225/3 = 75 for 30 nm biot-AuNPs, 625/3 = 208 for 50 nm biot-AuNPs, and 1600/3 = 533 for 80 nm biot-AuNP). (b−d) Selected PL decay curves detected within the Tb donor channel for increasing ratios of (x biot-AuNPs) per (y Tb-sAv): (b) 30 nm biot-AuNPs with y = 225 Tb-sAv; (c) 50 nm biot-AuNPs with y = 625 Tb-sAv; and (d) 80 nm biot-AuNPs with y = 1600 Tb-sAv. Black: x = 0; red: x = 0.2; orange: x = 0.5; green: x = 1; blue: x = 2; violet: x = 3; and pink: x = 4.

sites on the AuNPs (see Figure S5 for 200% amount of Tb-sAv added). The position of the maximum did not change over time before adding Tb-sAv, which was in line with the stability of the biot-AuNPs in the buffer. A prompt, small wavelength shift was observed in the light-scattering resonance of the biot-AuNPs when Tb-sAv was added to the solution. Subsequently, there was virtually no evolution of λ_{max} at longer times after adding Tb-sAv. The observed evolution of λ_{max} is consistent with the binding of Tb-sAv to the biot-AuNPs. The absence of changes in λ_{max} after binding of Tb-sAv to the biot-AuNPs indicates that no significant clustering of Tb-sAv/biot-AuNPs into multi-AuNP aggregates occurred, and that under the experimental conditions, the only donor−acceptor assemblies are based on single AuNPs.

The PL titration experiments (Figure 3) provided further insight into the interaction between Tb-sAv and biot-AuNPs. As the concentration of biot-AuNPs was increased in solutions of constant Tb-sAv concentration, the integrated time-gated Tb PL intensity decreased sharply (Figure 3a) until a certain concentration ratio, after which no further decrease took place. The decrease in the overall intensity was accompanied by the appearance of a short PL decay component in the Tb PL decay curves (Figure 3b−d) at the expense of the long-lived Tb decay from the initial Tb-sAv, which indicates energy transfer from Tb to AuNP.

The PL titration behavior can readily be interpreted in terms of the formation of Tb-sAv/biot-AuNP assemblies. Taking into account the results from the resonant light-scattering spectroscopy, we can infer that these assemblies exist as isolated biot-AuNPs, bearing one or more Tb-sAv entities. The concentration ratio [biot-AuNP]/[Tb-sAv] beyond which the PL intensity remains constant is the concentration ratio at which all (active) Tb-sAv are bound to biot-AuNP. This happened in all cases at approximately 3 times the initially estimated concentration of biot-AuNP necessary to bind all Tb-sAv. This common factor of 3 demonstrates the similarity in binding behavior of the four diameters of particles because the initial estimates were based on the same assumptions for each particle diameter. According to the PL titrations, the binding capacity was 2, 75, 208, and 533 Tb-sAv per biot-AuNP for 5, 30, 50, and 80 nm AuNPs, respectively. Using the surface areas of the different AuNPs (vide supra) and the size of sAv in the solid state (5.8 nm × 5.4 nm × 4.9 nm),[25] which would lead to a surface footprint of 24.6 nm^2 (π × 2.9 nm × 2.7 nm), the simple geometrical estimates for coverage of sAv per AuNP are 3 (5 nm AuNPs), 115 (30 nm AuNPs), 319 (50

DOI: 10.1021/acs.jpcc.8b06539
J. Phys. Chem. C 2018, 122, 17566−17574

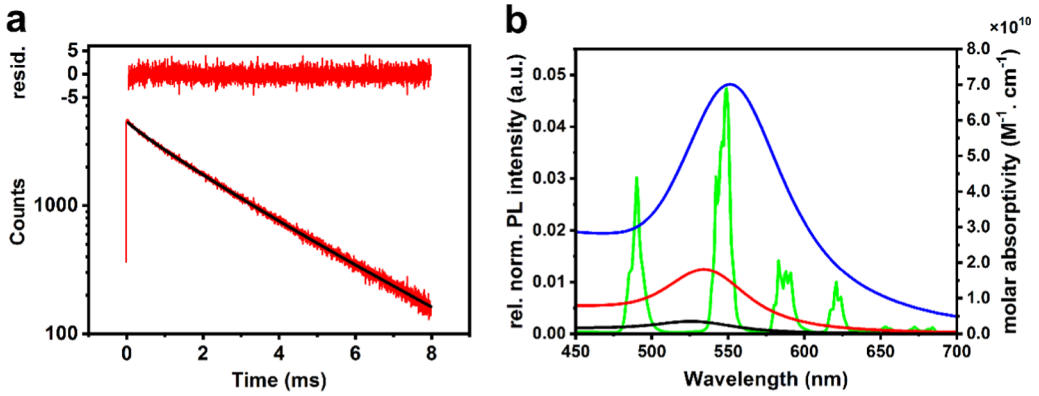

Figure 4. (a) PL decay (λ_{ex} = 337.1 nm; λ_{em} = (490 ± 20) nm) of Tb-sAv in buffer (red) and fit (black) using a single Kohlrausch (stretched exponential) decay law; yielding an average lifetime of $\langle\tau\rangle$ = 2.19 ms. On top: weighted residuals indicating a good fit between model and experimental data, reduced χ^2 = 1.26. (b) Overlap between extinction spectra of 30 nm (black), 50 nm (red), and 80 nm (blue) biot-AuNP acceptors and emission spectrum of the Tb-sAv donor (green). The extinction spectrum of 5 nm biotin AuNPs, which is very weak, is given in the Supporting Information (Figure S1).

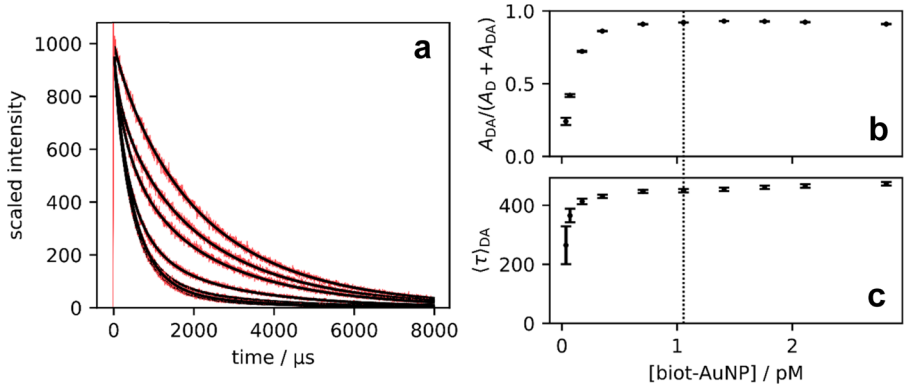

Figure 5. Analysis of PL decays of Tb-sAv (0.22 nM) in the presence of increasing amounts of 50 nm biot-AuNP in buffer. (a) Experimental decay traces (red), with fitted two-component Kohlrausch decay laws (black, eq 3). The traces were scaled to equal initial amplitude for clarity. (b) Amplitude fraction of the Tb-sAv/biot-AuNP donor−acceptor assembly PL decay in the total PL decay as a function of biot-AuNP concentration obtained from the curve fits. (c) Average PL decay times for the Tb-sAv/AuNP assemblies. The dotted line indicates the minimal biot-AuNP concentration to bind all available Tb-sAv (i.e., 208 Tb-sAv per biot-AuNP). The error bars indicate 95% confidence intervals.

nm AuNPs), and 817 (80 nm AuNPs). When taking into account the curved surface of the AuNPs, the hydration layer of sAv, and possible steric hindrance in sAv binding to biotin in very close proximity, the 35% lower values determined by PL titration are very close to full surface coverage in the simple geometric surface approximation. At [biot-AuNP]/[Tb-sAv] ratios below the equivalence point, biot-AuNPs carry the maximum number of Tb-sAv. At excess biot-AuNP compared to Tb-sAv, the number of Tb-sAv per biot-AuNP decreases.

Time-Resolved PL Decay Analysis. To investigate the energy-transfer mechanism in the Tb−AuNP assemblies, we analyzed the PL decay curves of solutions containing Tb-sAv and Tb-sAv/biot-AuNP assemblies. The PL decay of unbound Tb-sAv in buffer slightly deviates from monoexponentiality (Figure 4a), which can be attributed to the conjugation of several Tb complexes (∼4) per sAv. The heterogeneity in the local environment experienced by each Tb ion at the different sAv sites gives rise to a distribution of decay rates. A straightforward approach for analyzing the PL decay of such a heterogeneous system is to use a Kohlrausch ("stretched exponential") decay law, as it describes the overall relaxation of systems with an underlying distribution of relaxation rates using a minimal number of adjustable parameters.[31−33] The Kohlrausch decay law is given by eq 1.

$$I(t) = A \exp[-(t/\tilde{\tau})^{\beta}] \quad (1)$$

For β = 1, a monoexponential decay is obtained; the underlying distribution is then a Dirac function centered at the decay time constant. For β going from 1 toward 0, the underlying distribution becomes increasingly broad. The average decay time constant for a Kohlrausch decay law is given by eq 2, where Γ is the gamma function.[31]

$$\langle\tau\rangle = \tilde{\tau}\Gamma\left(1 + \frac{1}{\beta}\right) \quad (2)$$

The experimental PL decay of Tb-sAv in buffer is well described (Figure 4a) by the Kohlrausch decay law eq 2, with $\tilde{\tau}_D$ = 2.07 ms and β_D = 0.88, which yields average decay time $\langle\tau\rangle_D$ = 2.19 ms. This average decay constant is very close to the average decay constant obtained from a biexponential fit $\langle\tau\rangle_D$ = 2.2 ms, (Supporting Information, Figure S13). The advantage of using the Kohlrausch decay law is that it requires only three parameters to be optimized compared to four for a biexponential decay law. The close fit of this decay law to the data demonstrates its relevance for the analysis of non-exponential PL decays of Tb complexes coupled to proteins,

DOI: 10.1021/acs.jpcc.8b06539
J. Phys. Chem. C 2018, 122, 17566−17574

Table 1. Tb Donor and Tb-sAv/biot-AuNP Donor−Acceptor Decay Times Obtained from Fits of Decay Models to the Experimental Tb(III) Luminescence Decay[a]

	Kohlrausch decay model			multiexponential decay model		
AuNP diam. (nm)	$\langle\tau\rangle_D$ (ms)	$\langle\tau\rangle_{DA}$ (ms)	η	$\langle\tau\rangle_D$ (ms)	$\langle\tau\rangle_{DA}$ (ms)	η
5	2.17 (±0.02)	0.80 (±0.01)	0.63 (±0.01)	2.15 (±0.02)	0.81 (±0.02)	0.62 (±0.01)
30	2.23 (±0.02)	0.19 (±0.01)	0.91 (±0.01)	2.20 (±0.02)	0.31 (±0.02)	0.86 (±0.02)
50	2.20 (±0.02)	0.46 (±0.01)	0.79 (±0.01)	2.19 (±0.02)	0.47 (±0.01)	0.79 (±0.01)
80[b]	1.66 (±0.02)	0.14 (±0.02)	0.92 (±0.02)	1.78 (±0.02)	0.22 (±0.03)	0.87 (±0.02)

[a]Uncertainties are reported as 95% confidence intervals. [b]Measurements for 80 nm biot-AuNPs were done in pure water instead of buffer; the donor lifetime is slightly shorter in this solvent.

where a distribution of decay constants is expected and observed.

When biot-AuNPs are added to the solution, Tb-sAv/biot-AuNP donor−acceptor assemblies are formed, leading to a mixture of free (excess) Tb-sAv donors and Tb-sAv/biot-AuNP assemblies. The overall PL decay can thus be considered to be the sum of the individual decays of these two species, each described by a Kohlrausch decay, with the subscripts D and DA referring to the free donor and the donor−acceptor assemblies, respectively (eq 3).

$$I(t) = A_D \exp[-(t/\tilde{\tau}_D)^{\beta_D}] + A_{DA} \exp[-(t/\tilde{\tau}_{DA})^{\beta_{DA}}] \quad (3)$$

For the values of $\tilde{\tau}_D$ and β_D, we used the values obtained from the measurement of the pure Tb-sAv donor and keep these fixed throughout our analysis, leaving only A_D, A_{DA}, $\tilde{\tau}_{DA}$, and β_{DA} to be determined by curve fitting. This was achieved by fitting the model eq 3 to the data using the "lmfit" package[34] in Python by minimizing the sum-over-squares of the residuals with the Levenberg−Marquardt algorithm. The residual for each time bin was weighted by $1/\sqrt{N_{counts}}$, where N_{counts} is the number of photons counted in the time bin. Reduced χ^2 values for the fits obtained were in the range of 1.25−1.45.

The analysis of the PL decay titration of Tb-sAv with biot-Au50-NP is shown in Figure 5. In presence of increasing biot-AuNP concentrations, the PL decay of the Tb-sAv donor is gradually replaced with a shorter PL decay component. This shorter component is attributed to the PL of Tb-sAv attached to the biot-AuNPs.

From the fits of the model to the data, we obtained the amplitudes of the donor and the donor−acceptor assemblies (A_D resp. A_{DA}), as well as the kinetic parameters for the donor−acceptor assemblies, $\tilde{\tau}_{DA}$ and β_{DA}, as a function of 50 nm biot-AuNPs concentration. From $\tilde{\tau}_{DA}$ and β_{DA}, we obtained the average decay time constant $\langle\tau\rangle_{DA}$ using eq 2. The donor−acceptor amplitude A_{DA} and the average decay time $\langle\tau\rangle_{DA}$ are plotted in Figure 5b,c, as a function of biot-AuNPs concentration. The amplitude fraction of the signal of the Tb−AuNPs donor−acceptor assemblies gradually increased with increasing concentration of biot-AuNPs and reached a plateau near 0.9, indicating a small fraction of Tb-sAv that are inactive in terms of binding to biotin. The luminescence decay due to this nonbinding fraction contributes to the signal of the donor-only decay (described by amplitude A_D and lifetime $\langle\tau\rangle_D$) but does not affect the determination of lifetime $\langle\tau\rangle_{DA}$ of the donor−acceptor assembly in the curve fits because the model used effectively separates the donor and donor−acceptor contributions.

The average PL decay time of the donor−acceptor assemblies remains constant when excess biot-AuNPs is present, i.e., in the cases where only few Tb-sAv are attached to each biot-AuNP. In contrast, the PL decay becomes shorter when the density of Tb-sAv per biot-AuNPs is higher (conditions of excess Tb-sAv). We tentatively ascribe this to the energy-transfer interactions between Tb complexes at the surface of the nanoparticles at high Tb-sAv loading levels. Another, less likely, explanation may be that a dense packing of Tb-sAv at the biot-AuNP surface changes the structure of the poly(ethylene glycol) PEG−biotin ligand shell in such a way as to reduce the average distance between the Tb complexes and the AuNP surface. To avoid contributions of these effects at a high loading level, only the measurements at low loading (higher biot-AuNPs concentrations at which $\langle\tau\rangle_{DA}$ remains constant) are included in the energy-transfer analysis. In these cases, we are approaching the idealized situation where one Tb complex interacts purely with one AuNP.

Similar behavior was observed with the 5, 30, and 80 nm biot-AuNPs (Figures S10−S12). Using the analysis procedure based on the Kohlrausch decay law, we are able to find the average decay times $\langle\tau\rangle_{DA}$ of Tb(III) luminescence in the donor−acceptor complexes. The results of this Kohlrausch-decay analysis for all AuNP diameters have been collected in Table 1. We consider the average decay time constants for the Tb-sAv/biot-AuNP at low Tb-sAv loading (i.e., high biot-AuNPs concentrations) to evaluate the energy-transfer efficiency from the Tb complex to the gold nanoparticle using eq 4.

$$\eta = 1 - \frac{\langle\tau\rangle_{DA}}{\langle\tau\rangle_D} \quad (4)$$

In all cases, the energy-transfer efficiency was larger than 50% but less than 95%, leaving some Tb(III) luminescence available for detection. In spite of the giant oscillator strengths of the localized plasmon resonance, luminescence quenching is incomplete, and incorporation of photoluminescent entities into assemblies of plasmonic particles for fluorescence tracking and sensing purposes remains feasible.

In addition to the Kohlrausch decay model introduced here, the PL decay curves were analyzed with a multiexponential analysis (Supporting Information) that has been successfully applied in past studies for Tb-to-quantum dot FRET systems.[34−36] The multiexponential analysis led to similar results as the Kohlrausch analysis (see Table 1), indicating consistency between the two models. The Kohlrausch model has the advantage of carrying less adjustable parameters and providing a clearer separation between donor-only and donor−acceptor contributions to the overall luminescence decay.

Energy-Transfer Mechanism: FRET vs NSET. The energy-transfer efficiencies indicate that PL quenching takes place by nonradiative energy transfer, and also that this

DOI: 10.1021/acs.jpcc.8b06539
J. Phys. Chem. C 2018, 122, 17566−17574

Table 2. FRET Model Evaluation of Resonance Energy Transfer from Tb to AuNPs

	5 nm	30 nm	50 nm	80 nm
κ^2	2/3	2/3	2/3	2/3
Φ_D	0.64	0.64	0.64	0.64
n (refractive index)	1.35	1.35	1.35	1.35
$J(\lambda)$ (M^{-1} cm^{-1} nm^4)	6.9×10^{17}	1.6×10^{20}	9.3×10^{20}	4.4×10^{21}
R_0 (nm)	14.1	34.8	46.8	60.7

quenching is incomplete, leaving some emission to be detected. Gold nanoparticles are known to be efficient quenchers for luminophores very close to their surface,[35−38] and the mechanism for this quenching has been attributed to either FRET or NSET mechanism.[9,10,39,11−18] We therefore subjected our PL decay time results to both FRET and NSET theory with the aim of contributing to the understanding of the energy-transfer processes in assemblies of photoluminescent entities and plasmonic nanoparticles, particularly to find out which theory, FRET or NSET, makes the best predictions about energy transfer in these systems. The long-lived PL emission from Tb enables a clear distinction of Tb from other short-lived background PL while still being subject to electric dipole−dipole energy transfer.[40]

For the FRET model analysis, the overlap integral (J) and Förster distance (R_0) were calculated using eqs 5 and 6.

$$J = \int \bar{I}_D(\lambda)\varepsilon_A(\lambda)\lambda^4 d\lambda \tag{5}$$

where $\bar{I}_D(\lambda)$ is the area-normalized emission spectrum of the donor, $\varepsilon_A(\lambda)$ is the molar absorptivity spectrum of the acceptor in M^{-1} cm^{-1}, and λ is the wavelength in nm. Figure 4b shows the intensity-normalized (area under the emission spectrum from 450 to 700 nm normalized to unity) PL spectrum of Tb donor and the absorption spectra of the differently sized biot-AuNP acceptors (5, 30, 50, and 80 nm).

$$R_0 = 0.0211\ [\kappa^2 \Phi_D (n)^{-4} J(\lambda)]^{1/6}\ (\text{in nm}) \tag{6}$$

where κ^2 is the orientation factor ($\kappa^2 = 2/3$ due to dynamic averaging as found for other Tb-NP donor−acceptor systems),[24,41] Φ_D is the Tb-centered quantum yield of the Tb donor (0.64), and n is the refractive index of the surrounding medium. The molar extinction coefficients $\varepsilon_{AuNP}(\lambda)$ for gold nanoparticles were obtained from the extinction cross sections calculated with analytic Mie expressions.[42] These are known to have excellent agreement with experimentally determined cross sections.[27]

Förster distances (R_0) were calculated to be 14.1, 34.8, 46.8, and 60.7 nm (for 5, 30, 50, and 80 nm AuNPs, respectively) when using the refractive index of the aqueous buffer (Table 2) or 17.4, 43.1, 57.9, and 75.1 nm, when using the refractive index of gold (Table S5). To fit the FRET model to different sizes of AuNPs, Wu et al. have suggested to subtract the radius of the AuNPs from the R_0 values.[17] In our case, that would lead to R_0 distances of 11.6, 19.8, 21.8, and 20.7 nm when using the refractive index of the aqueous buffer and 14.9, 28.1, 32.9, and 35.1 nm when using the refractive index of gold. All R_0 values are far beyond the expected Tb-sAv/biot-AuNP distances, which provides a good evidence that the FRET mechanism is not operational here.

Within the FRET model, the Tb−AuNP distance (r) was calculated using eq 7.[5]

$$r = R_0 \left(\frac{\tau_{DA}}{\tau_D - \tau_{DA}} \right)^{1/6} \tag{7}$$

As shown in detail in Tables S6 and S7, the calculated distances between Tb and the AuNP surface globally range from 4.2 to 50.5 nm (excluding an unrealistic 0.8 nm value). The calculated distances span a very large range, with almost all values far beyond a distance that could be attained by the dimensions of the streptavidin−biotin pair separating the Tb donors from the gold nanosurface. Moreover, these calculated distances do not show much consistency between the results for 5, 30, 50, and 80 nm particles, and there is ambiguity in how to handle the fact that the AuNPs cannot be treated as a point dipole.

For the NSET analysis, R_0 was calculated by eq 8.[11,12]

$$R_0^{NSET} = \left[0.225 \frac{\Phi_D}{\omega_D} \frac{1}{\omega_F k_F} c^3 \right]^{1/4} \tag{8}$$

where ω_D is the angular frequency resonant with the donor electronic transition, ω_f and k_f are the angular frequency and the Fermi vector for bulk gold, respectively, and c is the speed of light. The calculated R_0^{NSET} was 7.2 nm for all four different sizes of AuNPs (Table 3). In NSET, R_0 is independent of the nanoparticle diameter because the energy transfer is assumed to be to a flat surface, which is a good approximation for a small emitting dipole in proximity to a much larger sphere.

Table 3. NSET Model Evaluation of Resonance Energy Transfer from Tb to AuNPs

c (m/s)	3×10^8
Φ_D	0.64
ω_D (s^{-1})	3.8×10^{15}
ω_F (s^{-1})	8.4×10^{15}
k_F (m^{-1})	1.2×10^{10}
R_0 (nm)	7.2

The Tb−AuNP distance (r) was subsequently calculated using eq 9.[5]

$$r = R_0^{NSET} \left(\frac{\tau_{DA}}{\tau_D - \tau_{DA}} \right)^{1/4} \tag{9}$$

With the PL decay times for the donor and the donor−acceptor assemblies as determined above, and the R_0 determined using the NSET theory, Tb−AuNP distances r were obtained and are collected in Table 4. All the distances found are in the 4.0−6.4 nm range and do not show a strong dependence on the acceptor AuNP diameter. Moreover, these distances are well in line with the estimated average distance of the Tb complexes conjugated randomly to the sAv binding via biotin to the surface of the AuNP (Figure 1).

DOI: 10.1021/acs.jpcc.8b06539
J. Phys. Chem. C 2018, 122, 17566−17574

Table 4. Tb−AuNP Surface Distances r Calculated from the Experimental Luminescence Decay Times and the NSET Theory[a]

AuNP diam. (nm)	Kohlrausch decay model		multiexponential decay model	
	r/R_0	r (nm)[b]	r/R_0	r (nm)[b]
5	0.87 (±0.01)	6.3 (±0.6)	0.88 (±0.01)	6.4 (±0.7)
30	0.55 (±0.01)	4.0 (±0.4)	0.63 (±0.03)	4.5 (±0.3)
50	0.72 (±0.01)	5.2 (±0.5)	0.72 (±0.01)	5.2 (±0.6)
80	0.55 (±0.02)	4.0 (±0.4)	0.62 (±0.03)	4.5 (±0.5)

[a]Distances were calculated from both Kohlrausch PL decay analysis and multiexponential decay results. [b]Using R_0 = 7.2 (±0.7) nm, assuming 10% uncertainty on R_0.

When considering the overall uncertainty on the donor−acceptor distances r derived from the experimental luminescence decay measurements, we distinguish two main sources of uncertainty, the first being the experimental error on the experimental decay times and the second being the uncertainty on the value on R_0^{NSET}. To separate these two contributions to the overall uncertainty, we have included the ratio r/R_0 in Table 4. This ratio thus depends solely on the uncertainty of the experimental measurements, which is relatively small. The uncertainty on R_0^{NSET} was estimated to be 10% and represents a systematic uncertainty. The NSET model afforded a set of donor−acceptor distances that are similar for various AuNP diameters studied and consistent with the expected structure of Tb-sAv/biot-AuNP assemblies.

CONCLUSIONS

We have demonstrated an efficient energy transfer between Tb donors and AuNP acceptors within different Tb-sAv/biot-AuNPs assemblies for AuNPs of 5, 30, 50, and 80 nm diameter. Characterization by RLS and time-resolved PL spectroscopy demonstrated the assembly of Tb-sAv/biot-AuNP with ratios up to 2 (5 nm AuNPs), 75 (30 nm AuNPs), 208 (50 nm AuNPs), and 533 (80 nm AuNPs) of Tb-sAv per biot-AuNP, in good agreement with the expectations based on the surface areas of the particles and the biotinylation density of the AuNPs. The stable Tb-sAv/biot-AuNP assemblies were investigated at different Tb-sAv per biot-AuNP ratios and AuNP sizes in aqueous solutions by time-resolved PL spectroscopy. The resulting PL decay curves were studied using both Kohlrausch (stretched exponential) and multiexponential PL lifetime models, which yielded mutually consistent results. The Kohlrausch method introduced here requires less fitting parameters and is therefore attractive for analysis of this type of donor−acceptor systems, in which a heterogeneity exists in the chemical environments of the luminescent species. The analyses showed that the energy-transfer efficiencies were independent of the AuNP size. In contrast to FRET, NSET theory provided a coherent analysis of the experimental energy-transfer results. The Tb donor to AuNP surface acceptor distances determined on the basis of NSET proved to be in excellent agreement with the structural conditions of the biotin-sAv binding on the AuNP surface. Our results present a strong evidence favoring NSET over FRET as the operational energy-transfer mechanism for the PL quenching of electric dipole emitters by AuNPs.

When comparing the quenching efficiencies predicted by NSET and by FRET, we find that NSET predicts less quenching for a given donor−acceptor distance, especially at shorter distance. This makes it more likely that fluorescence of fluorophores attached to plasmonic nanoparticles is partially retained and can still be useful for the detection of such assemblies. Moreover, successful design and optimization of biosensors such as "nano-flares"[19,20] and molecular rulers[10] based on AuNP PL quenching is clearly dependent on the understanding of the underlying energy-transfer mechanism, to which our study has contributed important findings in favor of NSET.

MATERIALS AND METHODS

Reagents. The biot-AuNPs were purchased from Sigma-Aldrich (5, 30, 50, and 80 nm diameter, biotin-terminated PEG mol wt 5000, dispersion in H_2O). For the measurements of 5, 30, and 50 nm AuNPs, 2 mM Tris−HCl (pH 8.5) was used as a solvent; for the measurements of 80 nm AuNPs, pure water was used as a solvent. Black Costar Half Area 96-well microtitration plates were purchased from Corning Inc. (Corning, NY), and Tb complexes (Lumi4-Tb) functionalized to sAv at a ratio of 4 Tb/sAv were provided by Lumiphore Inc. (Berkeley, CA).

Optimization of Buffer Conditions. Optical extinction and light-scattering spectra were measured on solutions of the biot-AuNPs in a selection of aqueous buffers. These spectroscopic measurements enabled to determine the long-term stability of biot-AuNPs in these buffers. Colloidal stability is a requirement for reliable results when forming donor−acceptor assemblies. Aggregation of unstable AuNPs would lead to clearly observable changes in the optical spectra. Light-scattering spectroscopy is particularly sensitive toward even slight changes in the chemical environment of plasmonic AuNPs.[27,28] From these measurements (see Figures S2−S4), it was concluded that 2−4 mM Tris−HCl buffer at pH 8.5 and pure water were the most suitable media for the experiments. An alternative buffer, phosphate-buffered saline (10 mM phosphate, pH 7.2, 137 mM NaCl, 2.7 mM KCl) also yielded stable nanoparticle solutions (no shift of the localized surface plasmon resonance maximum) but led to a more pronounced "sticking" of the biot-AuNPs to the walls of the spectroscopic cells.

Formation of Tb−AuNP Donor−Acceptor Assemblies. We used different but constant concentrations of Tb-sAv for the experiments with each of the four AuNPs. To these constant concentrations of Tb-sAv, increasing amounts of biot-AuNPs were added, such that the fraction of biot-AuNPs (x) was given per 6 Tb-sAv for 5 nm biot-AuNPs (25/4 = 6; 25 biotins on 4 sAv binding sites), per 225 Tb-sAv for 30 nm biot-AuNPs (900/4 = 225), per 625 Tb-sAv for 50 nm biot-AuNPs (2500/4 = 625), and per 1600 Tb-sAv for 80 nm biot-AuNPs (6400/4 = 1600). Tb-sAv was dissolved to 20.7 μM in anhydrous dimethylformamide, which corresponded to 82.8 μM of Tb (conjugation ratio of 4 Tb/sAv). For 5 nm biot-AuNPs, Tb-sAv was diluted to 2.73 nM in pure water. For the total measuring volume of 150 μL, 50 μL of Tb-sAv solutions was mixed with 100 μL of biot-AuNP solutions containing increasing amounts (0, 1, 5, 10, 20, 30, 40, 50, 60, 70, and 80 μL) of 5 nm biot-AuNPs (9.09 nM) in 2 mM Tris−HCl buffer at pH 8.5. The mixtures were incubated for 2 h at 37 °C. For 30 nm biot-AuNPs, Tb-sAv was diluted to 1.33 nM in pure water. For the total measuring volume of 150, 50 μL of Tb-sAv solutions was mixed with 100 μL of biot-AuNP solutions containing increasing amounts (0, 1, 2, 5, 10, 20, 30, 40, 50, 60, and 80 μL) of 30 nm biot-AuNPs (29.6 pM) in 2 mM Tris−

DOI: 10.1021/acs.jpcc.8b06539
J. Phys. Chem. C 2018, 122, 17566−17574

HCl buffer at pH 8.5. The mixtures were incubated for 2 h at 37 °C. For 50 nm biot-AuNPs, Tb-sAv was diluted to 0.65 nM in pure water. For the total measuring volume of 150 μL, 50 μL of Tb-sAv solutions was mixed with 100 μL of biot-AuNP solutions containing increasing amounts (0, 1, 2, 5, 10, 20, 30, 40, 50, 60, and 80 μL) of 50 nm biot-AuNPs (5.3 pM) in 2 mM Tris−HCl buffer at pH 8.5. The mixtures were incubated for 2 h at 37 °C. For 80 nm biot-AuNPs, Tb-sAv was diluted to 0.72 nM in pure water. For the total measuring volume of 150, 50 μL of Tb-sAv solutions was mixed with 100 μL of biot-AuNP solutions containing increasing amounts (0, 1, 2, 5, 10, and 20 μL) of 80 nm biot-AuNPs (2.24 pM) in pure water. The mixtures were incubated while shaking slowly overnight at room temperature.

Analytical Methods. Extinction spectra were acquired using a Lambda 35 UV−vis spectrophotometer from Perkin Elmer or on a modular fiber-based spectrometer system (OceanOptics LS-1 white light source and USB4000-VIS−NIR CCD spectrometer). Resonant light-scattering spectroscopy (RLS) of the AuNP and AuNP−Tb-sAv solutions was performed using a fiber-coupled incandescent white light source (AvaLight-HAL-(S)-mini) and an OceanOptics QE65000 spectrograph, at right angle, using our published method,[27,28,43] A 200× diluted Ludox solution[44] in 50 mM aqueous NaCl was used as the reference. The corrected light-scattering spectra represent the relative light-scattering cross sections as a function of wavelength.

In the kinetics experiments probing the stability of the biot-AuNP solutions and the binding of Tb-sAv/biot-AuNP, corrected light-scattering spectra were recorded at evenly spaced time intervals (rate typically 1 spectrum per 10 s). The position of the maximum of the resonant light-scattering band λ_{max}^{RLS} in each recorded spectrum was determined by fitting a parabola through the data points in a narrow spectral window ($\Delta\lambda$ = 10 nm) around the numerical maximum. The maximum of the parabola obtained from this first fit was then used as the center point for a second parabolic fit through the measured spectral data points over a narrow window ($\Delta\lambda$ = 10 nm), from which a refined determination of the position of the maximum was deduced. This procedure yielded stable and reproducible measurement of the position of the resonant light-scattering maximum λ_{max}^{RLS} and mitigates problems due to noise on the measured spectrum.

For the measurement of the PL decay curves of the Tb−AuNPs, an EI fluorescence plate reader (Edinburgh Instruments, U.K.) was used. For the multichannel scaler, 4000 detection bins of 2 μs integration time were used. A nitrogen laser (LTB, Berlin, Germany) was used for excitation (337.1 nm, 20 Hz, 600 flashes). A 494 ± 20 nm bandpass filter was used for analyzing the Tb PL. Multiexponential fits to the data were done with FAST software version 3.1 (Edinburgh Instruments, U.K.). Kohlrausch decay analysis was done using the Python programming language and the lmfit package.[34] All the assays were measured in black 96-well microtiter plates with an optimal working volume of 150 μL.

■ ASSOCIATED CONTENT

Supporting Information

The Supporting Information is available free of charge on the ACS Publications website at DOI: 10.1021/acs.jpcc.8b06539.

Stability of the AuNPs in buffer (Figures S2−S4) and in the presence of excess sAv (Figure S5), time-resolved PL decays of Tb-sAv/biot-AuNP assemblies (Figures S6−S9), Kohlrausch stretched exponential analysis of Tb PL decays for 5, 30, and 80 nm AuNPs (Figures S10−S12), multiexponential PL decay analysis (Figure S13, Tables S1−S4), and additional FRET investigations (Tables S5 and S7) (PDF)

■ AUTHOR INFORMATION

Corresponding Authors

*E-mail: niko.hildebrandt@u-psud.fr (N.H.).
*E-mail: martinus.werts@ens-rennes.fr (M.H.V.W.).

ORCID

Chi Chen: 0000-0002-6126-1824
Niko Hildebrandt: 0000-0001-8767-9623
Martinus H. V. Werts: 0000-0003-1965-8876

Author Contributions

§C.C. and C.M. contributed equally to this work.

Notes

The authors declare no competing financial interest.

■ ACKNOWLEDGMENTS

The authors thank Lumiphore, Inc. for the gift of Lumi4 reagents and Dr. J. M. Zwier for stimulating discussions concerning the Kohlrausch stretched exponential decay function. This work was partially funded by Agence Nationale de la Recherche (grant ANR-2010-JCJC-1005-1, "COMON-SENS") and the European Commission (H2020 FET-Open project PROSEQO). C.M. and M.H.V.W. acknowledge financial support from Région Bretagne and ENS Rennes (ARED Ph.D. programme, project "ELFENOR"). C.C. acknowledges the IDEX Paris-Saclay (Investissements d'avenir) for his PhD fellowship. N.H. acknowledges the Institut Universitaire de France (IUF) for financial support.

■ REFERENCES

(1) Selvin, P. R. The Renaissance of Fluorescence Resonance Energy Transfer. *Nat. Struct. Biol.* **2000**, *7*, 730−734.
(2) Ha, T. Single-Molecule Fluorescence Resonance Energy Transfer. *Methods* **2001**, *25*, 78−86.
(3) Weiss, S. Measuring Conformational Dynamics of Biomolecules by Single Molecule Fluorescence Spectroscopy. *Nat. Struct. Biol.* **2000**, *7*, 724−729.
(4) Clapp, A. R.; Medintz, I. L.; Mauro, J. M.; Fisher, B. R.; Bawendi, M. G.; Mattoussi, H. Fluorescence Resonance Energy Transfer Between Quantum Dot Donors and Dye-Labeled Protein Acceptors. *J. Am. Chem. Soc.* **2004**, *126*, 301−310.
(5) Medintz, I.; Hildebrandt, N. *FRET—Förster Resonance Energy Transfer*; Medintz, I., Hildebrandt, N., Eds.; Wiley-VCH Verlag GmbH & Co. KGaA: Weinheim, Germany, 2013.
(6) Sekar, R. B.; Periasamy, A. Fluorescence Resonance Energy Transfer (FRET) Microscopy Imaging of Live Cell Protein Localizations. *J. Cell Biol.* **2003**, *160*, 629−633.
(7) Persson, B. N. J.; Lang, N. D. Electron-Hole-Pair Quenching of Excited States near a Metal. *Phys. Rev. B* **1982**, *26*, 5409−5415.
(8) Samanta, A.; Zhou, Y.; Zou, S.; Yan, H.; Liu, Y. Fluorescence Quenching of Quantum Dots by Gold Nanoparticles: A Potential Long Range Spectroscopic Ruler. *Nano Lett.* **2014**, *14*, 5052−5057.
(9) Pons, T.; Medintz, I. L.; Sapsford, K. E.; Higashiya, S.; Grimes, A. F.; English, D. S.; Mattoussi, H. On the Quenching of Semiconductor Quantum Dot Photoluminescence by Proximal Gold Nanoparticles. *Nano Lett.* **2007**, *7*, 3157−3164.
(10) Yun, C. S.; Javier, A.; Jennings, T.; Fisher, M.; Hira, S.; Peterson, S.; Hopkins, B.; Reich, N. O.; Strouse, G. F. Nanometal

Surface Energy Transfer in Optical Rulers, Breaking the FRET Barrier. *J. Am. Chem. Soc.* **2005**, *127*, 3115−3119.
(11) Jennings, T. L.; Schlatterer, J. C.; Singh, M. P.; Greenbaum, N. L.; Strouse, G. F. NSET Molecular Beacon Analysis of Hammerhead RNA Substrate Binding and Catalysis. *Nano Lett.* **2006**, *6*, 1318−1324.
(12) Jennings, T. L.; Singh, M. P.; Strouse, G. F. Fluorescent Lifetime Quenching near d = 1.5 Nm Gold Nanoparticles: Probing NSET Validity. *J. Am. Chem. Soc.* **2006**, *128*, 5462−5467.
(13) Chen, Y.; O'Donoghue, M. B.; Huang, Y.-F.; Kang, H.; Phillips, J. A.; Chen, X.; Estevez, M.-C.; Yang, C. J.; Tan, W. A Surface Energy Transfer Nanoruler for Measuring Binding Site Distances on Live Cell Surfaces. *J. Am. Chem. Soc.* **2010**, *132*, 16559−16570.
(14) Zhang, X.; Marocico, C. A.; Lunz, M.; Gerard, V. A.; Gun'Ko, Y. K.; Lesnyak, V.; Gaponik, N.; Susha, A. S.; Rogach, A. L.; Bradley, A. L. Wavelength, Concentration, and Distance Dependence of Nonradiative Energy Transfer to a Plane of Gold Nanoparticles. *ACS Nano* **2012**, *6*, 9283−9290.
(15) Saraswat, S.; Desireddy, A.; Zheng, D.; Guo, L.; Lu, H. P.; Bigioni, T. P.; Isailovic, D. Energy Transfer from Fluorescent Proteins to Metal Nanoparticles. *J. Phys. Chem. C* **2011**, *115*, 17587−17593.
(16) Kapur, A.; Aldeek, F.; Ji, X.; Safi, M.; Wang, W.; Del Cid, A.; Steinbock, O.; Mattoussi, H. Self-Assembled Gold Nanoparticle-Fluorescent Protein Conjugates as Platforms for Sensing Thiolate Compounds via Modulation of Energy Transfer Quenching. *Bioconjugate Chem.* **2017**, *28*, 678−687.
(17) Li, M.; Cushing, S. K.; Wang, Q.; Shi, X.; Hornak, L. A.; Hong, Z.; Wu, N. Size-Dependent Energy Transfer between CdSe/ZnS Quantum Dots and Gold Nanoparticles. *J. Phys. Chem. Lett.* **2011**, *2*, 2125−2129.
(18) Guo, W.; Wei, Y.; Dai, Z.; Chen, G.; Chu, Y.; Zhao, Y. Nanostructure and Corresponding Quenching Efficiency of Fluorescent DNA Probes. *Materials* **2018**, *11*, No. 272.
(19) Li, N.; Chang, C.; Pan, W.; Tang, B. A Multicolor Nanoprobe for Detection and Imaging of Tumor-Related MRNAs in Living Cells. *Angew. Chem., Int. Ed.* **2012**, *51*, 7426−7430.
(20) Vilela, P.; Heuer-Jungemann, A.; El-Sagheer, A.; Brown, T.; Muskens, O. L.; Smyth, N. R.; Kanaras, A. G. Sensing of Vimentin MRNA in 2D and 3D Models of Wounded Skin Using DNA-Coated Gold Nanoparticles. *Small* **2018**, *14*, No. 1703489.
(21) Zhong, Y.; Zeng, F.; Chen, J.; Wu, S.; Hou, C.; Tong, Z. Modulation of Fluorescence of a Terbium-Complex-Containing Polymer by Gold Nanoparticles through Energy Transfer. *J. Inorg. Organomet. Polym. Mater.* **2007**, *17*, 679−685.
(22) Comby, S.; Gunnlaugsson, T. Luminescent Lanthanide-Functionalized Gold Nanoparticles: Exploiting the Interaction with Bovine Serum Albumin for Potential Sensing Applications. *ACS Nano* **2011**, *5*, 7184−7197.
(23) Ipe, B. I.; Yoosaf, K.; Thomas, K. G. Functionalized Gold Nanoparticles as Phosphorescent Nanomaterials and Sensors. *J. Am. Chem. Soc.* **2006**, *128*, 1907−1913.
(24) Hildebrandt, N.; Wegner, K. D.; Algar, W. R. Luminescent Terbium Complexes: Superior Förster Resonance Energy Transfer Donors for Flexible and Sensitive Multiplexed Biosensing. *Coord. Chem. Rev.* **2014**, *273*−*274*, 125−138.
(25) Hendrickson, W. A.; Pähler, A.; Smith, J. L.; Satow, Y.; Merritt, E. A.; Phizackerley, R. P. Crystal Structure of Core Streptavidin Determined from Multiwavelength Anomalous Diffraction of Synchrotron Radiation. *Proc. Natl. Acad. Sci. U.S.A.* **1989**, *86*, 2190−2194.
(26) Geißler, D.; Charbonnière, L. J.; Ziessel, R. F.; Butlin, N. G.; Löhmannsröben, H. G.; Hildebrandt, N. Quantum Dot Biosensors for Ultrasensitive Multiplexed Diagnostic. *Angew. Chem., Int. Ed.* **2010**, *49*, 1396−1401.
(27) Navarro, J. R. G.; Werts, M. H. V. Resonant Light Scattering Spectroscopy of Gold, Silver and Gold-silver Alloy Nanoparticles and Optical Detection in Microfluidic Channels. *Analyst* **2013**, *138*, 583−592.
(28) Loumaigne, M.; Midelet, C.; Doussineau, T.; Dugourd, P.; Antoine, R.; Stamboul, M.; Débarre, A.; Werts, M. H. V. Optical Extinction and Scattering Cross Sections of Plasmonic Nanoparticle Dimers in Aqueous Suspension. *Nanoscale* **2016**, *8*, 6555−6570.
(29) Englebienne, P. Use of Colloidal Gold Surface Plasmon Resonance Peak Shift to Infer Affinity Constants from the Interactions between Protein Antigens and Antibodies Specific for Single or Multiple Epitopes. *Analyst* **1998**, *123*, 1599−1603.
(30) Ghosh, S. K.; Pal, T. Interparticle Coupling Effect on the Surface Plasmon Resonance of Gold Nanoparticles: From Theory to Applications. *Chem. Rev.* **2007**, *107*, 4797−4862.
(31) Berberan-Santos, M. N.; Bodunov, E. N.; Valeur, B. Mathematical Functions for the Analysis of Luminescence Decays with Underlying Distributions 1. Kohlrausch Decay Function (Stretched Exponential). *Chem. Phys.* **2005**, *315*, 171−182.
(32) Johnston, D. C. Stretched Exponential Relaxation Arising from a Continuous Sum of Exponential Decays. *Phys. Rev. B* **2006**, *74*, No. 184430.
(33) Zwier, J. M.; Van Rooij, G. J.; Hofstraat, J. W.; Brakenhoff, G. J. Image Calibration in Fluorescence Microscopy. *J. Microsc.* **2004**, *216*, 15−24.
(34) Newville, M.; Ingargiola, A.; Stensitzki, T.; Allen, D. B. *Lmfit: Non-Linear Least-Square Minimization and Curve-Fitting for Python*; Astrophysics Source Code Library, 2014.
(35) Loumaigne, M.; Praho, R.; Nutarelli, D.; Werts, M. H. V.; Débarre, A. Fluorescence Correlation Spectroscopy Reveals Strong Fluorescence Quenching of FITC Adducts on PEGylated Gold Nanoparticles in Water and the Presence of Fluorescent Aggregates of Desorbed Thiolate Ligands. *Phys. Chem. Chem. Phys.* **2010**, *12*, 11004−11014.
(36) Navarro, J. R. G.; Plugge, M.; Loumaigne, M.; Sanchez-Gonzalez, A.; Mennucci, B.; Débarre, A.; Brouwer, A. M.; Werts, M. H. V. Probing the Interactions between Disulfide-Based Ligands and Gold Nanoparticles Using a Functionalised Fluorescent Perylene-Monoimide Dye. *Photochem. Photobiol. Sci.* **2010**, *9*, 1042−1054.
(37) Nerambourg, N.; Praho, R.; Werts, M. H. V.; Thomas, D.; Blanchard-Desce, M. Hydrophilic Monolayer-Protected Gold Nanoparticles and Their Functionalisation with Fluorescent Chromophores. *Int. J. Nanotechnol.* **2008**, *5*, 722−740.
(38) Huang, T.; Murray, R. W. Quenching of $[Ru(Bpy)_3]^{2+}$ Fluorescence by Binding to Au Nanoparticles. *Langmuir* **2002**, *18*, 7077−7081.
(39) Ji, X.; Wang, W.; Mattoussi, H. Controlling the Spectroscopic Properties of Quantum Dots via Energy Transfer and Charge Transfer Interactions: Concepts and Applications. *Nano Today* **2016**, *11*, 98−121.
(40) Selvin, P. R.; Hearst, J. E. Luminescence Energy Transfer Using a Terbium Chelate: Improvements on Fluorescence Energy Transfer. *Proc. Natl. Acad. Sci. U.S.A.* **1994**, *91*, 10024−10028.
(41) Hildebrandt, N.; Spillmann, C. M.; Algar, W. R.; Pons, T.; Stewart, M. H.; Oh, E.; Susumu, K.; Díaz, S. A.; Delehanty, J. B.; Medintz, I. L. Energy Transfer with Semiconductor Quantum Dot Bioconjugates: A Versatile Platform for Biosensing, Energy Harvesting, and Other Developing Applications. *Chem. Rev.* **2017**, *117*, 536−711.
(42) Bohren, C. F.; Huffman, D. R. *Absorption and Scattering of Light by Small Particles*; Willey-VCH: New York, 1998, p 541.
(43) Midelet, J.; El-Sagheer, A. H.; Brown, T.; Kanaras, A. G.; Débarre, A.; Werts, M. H. V. Spectroscopic and Hydrodynamic Characterisation of DNA-Linked Gold Nanoparticle Dimers in Solution Using Two-Photon Photoluminescence. *ChemPhysChem* **2018**, *19*, 827−836.
(44) Deželić, G.; Kratohvil, J. P. Determination of Size of Small Particles by Light Scattering. Experiments on Ludox Colloidal Silica. *Kolloid-Z.* **1960**, *173*, 38−48.

DOI: 10.1021/acs.jpcc.8b06539
J. Phys. Chem. C 2018, 122, 17566−17574